ARCHIVES OF ELECTRICAL ENGINEERING VOL. 71(1), pp. 159–174 (2022)

DOI 10.24425/aee.2022.140203

Analysis of electromagnetic performance of the interior permanent magnet brushless DC motor with stator slot skewed structure based on quasi-3D moving electromagnetic-field circuit coupling calculation

XUE-GUI GAN[1], ZHEN-NAN FAN[1] ✉, JING-CAN LI[2]

[1] *The Key Laboratory of Fluid and Power Machinery, Ministry of Education, Xihua University Chengdu, China*

[2] *State Key Laboratory of Power Transmission Equipment & System Security and New Technology Chongqing University Chongqing, China*

e-mail: xuegui_gan@163.com, {lijingcan_cqu/✉fanzhennan}@126.com

(Received: 23.07.2021, revised: 11.10.2021)

Abstract: This paper takes a 50 kW interior permanent magnet brushless DC motor as an example, and explores the influence of the degree of stator slot skew on the overall motor magnetic density and air gap magnetic density; then reveals the influences of stator slot skewed structure on a series of key electromagnetic properties like no-load back electromotive force (B-EMF), cogging torque, electromagnetic torque, torque fluctuation, electromagnetic loss, input power, output power and operating efficiency. On this basis, a relatively best range of the skew degrees is obtained. The research work in this paper has direct reference value for the further improvement of design and manufacture, operation and maintenance, control and protection of such motors.

Key words: interior permanent magnet brushless DC motor, quasi-three-dimensional electromagnetic-field circuit coupling analysis, stator slot skew

1. Introduction

As an excellent electric drive device, the interior permanent magnet brushless DC motor has a series of advantages such as compact size, high efficiency, wide speed regulation area, and high-speed regulation accuracy [1, 2]. In recent years, it has been widely used and developed in many fields such as electrical automation, medical equipment, aerospace.

However, due to the existence of the cogging effect, once the electromagnetic analysis design of the motor is improper, it may face a series of problems such as excessive cogging torque, obvious electromagnetic torque ripple, deterioration of no-load potential waveform, and reduced operating efficiency. It would not only cause the adverse influence for the quality of motor operation control, but also possibly lead to motor operation failures, even economic losses and safety threats. Therefore, in order to overcome the above shortcomings, it is necessary to evaluate and optimize the electromagnetic structure of this type of motor from the perspective of motor physical field modeling and analysis. In this regard, for a long time, domestic and foreign researchers have achieved a number of constructive results, including the optimization of air gap length, permanent magnet thickness, slot conjunction, pole arc coefficient, etc. [3, 4]; improved measures to reduce the torque ripple of surface-mounted permanent magnet synchronous motors by adopting different rotor pole skew methods [6]; the optimal design of the interior permanent magnet brushless DC motor by using permanent magnet segmented structure [7]; the loss mechanism of harmonic and slotting effects of the interior permanent-magnet (IPM) motor [8], and more.

However, up to now, stator slot skew structure is a classical method for optimizing electromagnetic performance [9]. Although some constructive research results have revealed its influence on the no-load B-EMF waveform, cogging torque, overload performance, and axial electromagnetic force for speed-regulating permanent magnet synchronous motors, for interior permanent magnet brushless DC motors, the influence of the stator slot skew structure on a series of key electromagnetic performance indicators such as cogging torque, B-EMF, torque ripple, electromagnetic power, operating efficiency, electromagnetic loss, etc., still needs to be researched in depth [10, 13, 14].

Therefore, this paper takes a 50 kW interior permanent magnet brushless DC motor as a research example. Aiming at the stator slot skew structure, based on the motor electromagnetic field theory and circuit theory, this paper established a quasi-three-dimensional electromagnetic-field circuit coupling analysis model, solved the electromagnetic field characteristics of this type of motor corresponding to different stator slot skew degrees, obtained the influence curve of the stator slot skew degree on the above-mentioned electromagnetic performance, and revealed the relevant electromagnetic structure design laws.

2. Calculation model

2.1. Basic motor parameters and selection of solving region

The basic parameters of the motor calculation example are shown in Table 1.

In terms of the research sample of the degree of stator slot skew, the variation range of the degree of skew in this paper is from 0 to 2 per stator slot pitch (t_1), and the change step is 0.1 per stator slot pitch ($0.1t_1$). In the calculation and analysis, the stator current remains constant and does not change with the degree of the skew.

In order to improve the efficiency of electromagnetic field analysis and solution in this paper according to the periodicity of the electromagnetic field distribution of the motor, a magnetic pole range is selected as the electromagnetic field solution area, so that the motor could be divided into 3 layers along the motor axis to consider the quasi-three-dimensional structure of the stator slot skew, as shown in Fig. 1.

Table 1. Basic parameters of the motor

Basic parameters	**Value**
Rated power	50 kW
Rated voltage	500 V
Rated speed	1200 rpm/min
Stator slot number	48
Rotor pole number	4
Winding	3-phase wye connected
Material of permanent magnet	NdFeB
Stator outer radius	141 mm
Rotor inner radius	56 mm

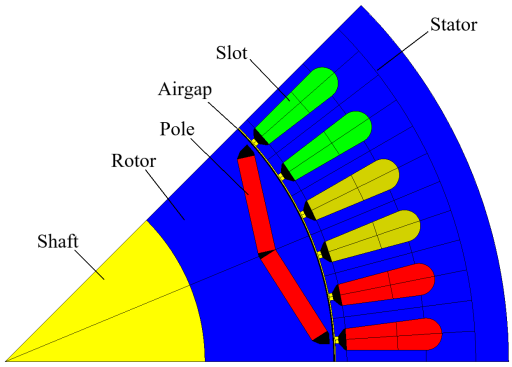

(a)

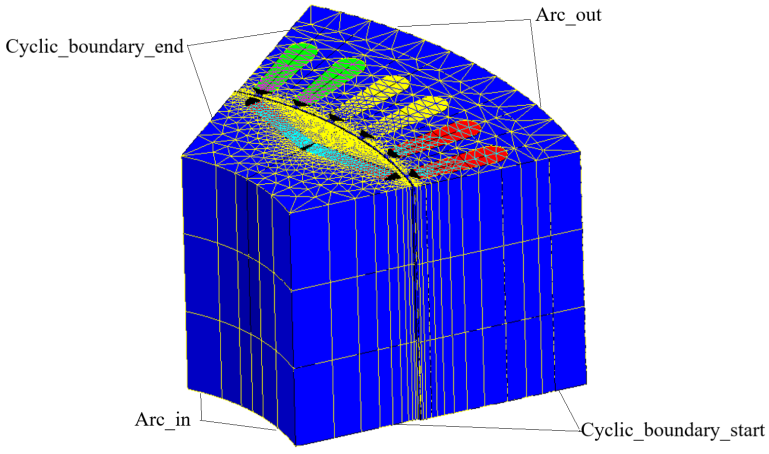

(b)

Fig. 1. 1/8 of the model of the motor

2.2. 3D multi-slice time-varying nonlinear moving electromagnetic-circuit field coupling model of the motor

Introducing the vector magnetic potential A, and considering the 3D structure of the stator slot skew, the 3D boundary value problem of the time-varying nonlinear moving electromagnetic field of this type of motor can be expressed as:

$$\begin{cases} \nabla \times (v\nabla \times A) + \dfrac{1}{\rho}\left[\dfrac{\partial A}{\partial t} - V \times (\nabla \times A)\right] = J_s \\ A|_{\text{Arc\_in}} = A|_{\text{Arc\_out}} \\ A|_{\text{Ccylic\_boundary\_start}} = -A|_{\text{Ccylic\_boundary\_end}} \end{cases} . \tag{1}$$

In the formula, J_{sz} is the imposed source current density, v is the magnetoresistance, V is the rotor rotation speed, and ρ is the resistivity.

For each layer, assuming that the current density and vector magnetic potential have only the z-axis component, and the velocity has only the x-axis component, introducing the Coulomb norm $\nabla \cdot \boldsymbol{A} = 0$, the boundary value problem of the time-varying nonlinear moving electromagnetic field can be transformed into a 2D expression:

$$\begin{cases} \dfrac{\partial}{\partial x}\left(v\dfrac{\partial A_{slz}}{\partial x}\right) + \dfrac{\partial}{\partial y}\left(v\dfrac{\partial A_{slz}}{\partial y}\right) = -J_{slz} + \dfrac{1}{\rho}\dfrac{\partial A_{slz}}{\partial t} + \dfrac{V_x}{\rho}\dfrac{\partial A_{slz}}{\partial x} \\ A\big|_{\text{Arc\_in}} = A\big|_{\text{Arc\_out}} \\ A\big|_{\text{Ccylic\_boundary\_start}} = -A\big|_{\text{Ccylic\_boundary\_end}} \end{cases} . \tag{2}$$

In this formula, A_{slz} is the z-axis component of the vector magnetic potential, J_{slz} is the z-axis component of the imposed source current density, and V_x is the x-axis component of the velocity.

Meanwhile, this paper established the circuit model of this motor as shown in Fig. 2.

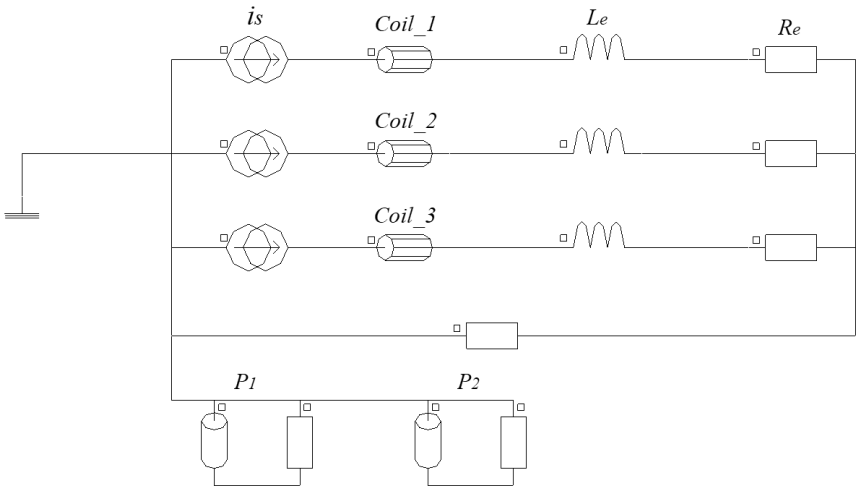

Fig. 2. Stator winding coupling circuit

In Fig. 2, i_s states for the constant current sources which represent the stator input current, *Coil*_1, *Coil*_2, *Coil*_3 are the winding coils, R_e and L_e are the winding leakage resistance and leakage inductance, respectively, finally, P_1 and P_2 are the coupling circuit elements which represent permanent magnets.

Combining the above-mentioned boundary value problem equation of the motor electromagnetic field and the motor circuit equation together constitutes a quasi-3D layered time-varying nonlinear electromagnetic-circuit field coupling model of this motor.

On this basis, according to the solution of the time-step finite element method, we could obtain a series of key electromagnetic performance parameters like the motor electromagnetic field, no-load B-EMF, cogging torque, electromagnetic torque, electromagnetic torque fluctuation, electromagnetic loss, input power, output power and operation efficiency.

3. Calculation results and analysis

3.1. Influence of motor magnetic field distribution on stator slot skew structure

Under the no-load condition, corresponding to the motor being in the generator mode, the calculation results of the magnetic density distribution for part of the stator slot skew structure scheme are shown in Fig. 3 and Fig. 4.

It can be seen from the above figure that when the stator straight slot structure is adopted, whether the overall magnetic density of the motor or the air gap magnetic density, no significant changes occur along the axis, as shown in Fig. 3(a) and Fig. 4(a). After adopting the stator slot skew structure, the above two types of magnetic density will change significantly along the motor axis, as shown in Fig. 3(b)–3(f) and Fig. 4(b)–4(f). Among them, with the change of the stator slot skew degree, both the overall magnetic density of the motor and the air gap magnetic density have different distribution with a certain regularity.

Moreover, no-load B-EMF and cogging torque of the motor is a function of the air-gap flux distribution. From the above figures, stator slot skew structure affectively changed the distribution of both the overall magnetic density of the motor and the air gap magnetic density, so it is necessary to analyze the influence of no-load B-EMF and cogging torque under different skew degrees.

3.2. Influence of no-load B-EMF and cogging torque for stator slot skew structure

This paper introduces the sinusoidal distortion rate of the waveform, which is used to describe the degree of deviation between the no-load B-EMF waveform and the standard sine waveform, and is used to measure the quality of the no-load induced voltage waveform [15]:

$$K_u = \frac{\sqrt{U_2^2 + U_3^2 + \ldots + U_n^2}}{U_1} \times 100\%. \tag{3}$$

In the formula: U_1 is the basic RMS value of the no-load B-EMF; U_n is the RMS value of the n-th harmonic of the no-load B-EMF, K_u is the deviation between the basic and sinusoidal waveforms of the RMS voltage.

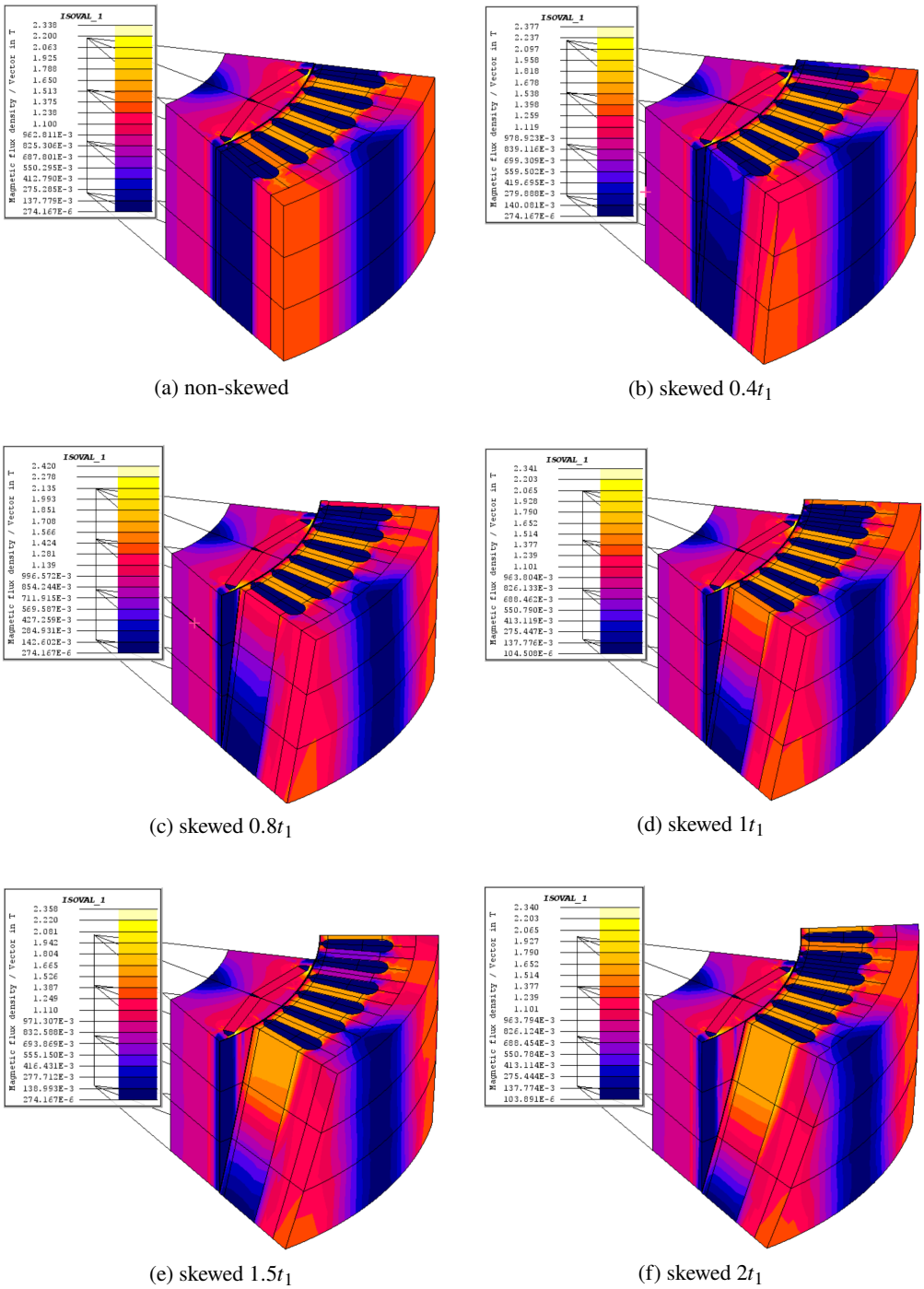

(a) non-skewed (b) skewed $0.4t_1$

(c) skewed $0.8t_1$ (d) skewed $1t_1$

(e) skewed $1.5t_1$ (f) skewed $2t_1$

Fig. 3. Motor magnetic density distribution map under different stator skew degree

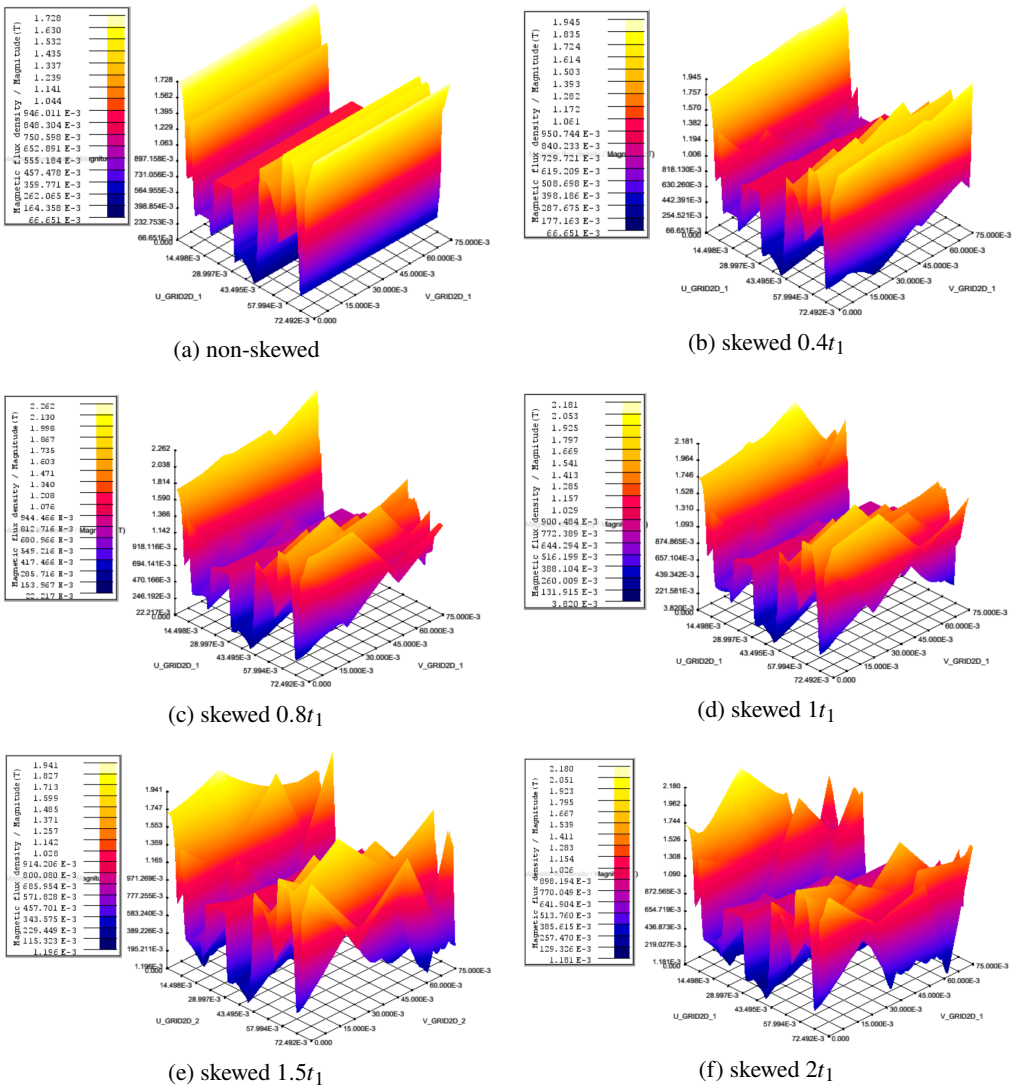

(a) non-skewed

(b) skewed $0.4t_1$

(c) skewed $0.8t_1$

(d) skewed $1t_1$

(e) skewed $1.5t_1$

(f) skewed $2t_1$

Fig. 4. Motor air gap flux density distribution map under different stator skew degree

The period of the cogging torque graph depends on the motor slot-pole-combination. This paper has computed the cogging torque over several periods to fully assess the stator teeth interaction with the rotor poles, and the time ranging of this model is selected for 0–45 s.

In this paper, the calculation results of no-load B-EMF and cogging torque corresponding to different stator skew degrees are shown in Figs. 5–8.

From the above results:

1. As far as the quality of the no-load B-EMF waveform is concerned, as shown in Fig. 5 and Fig. 6, its waveform sinusoidal distortion rate decreases with the increase of the stator slot

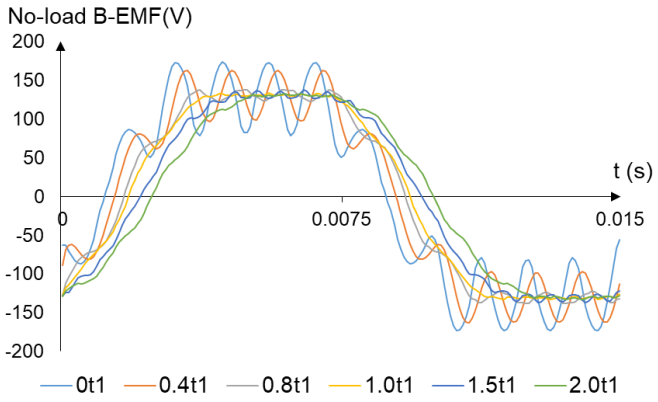

Fig. 5. No-load B-EMF waveform corresponding to part of the skew scheme

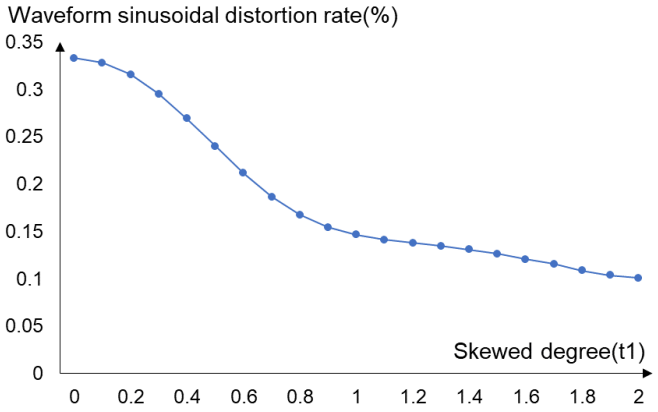

Fig. 6. Waveform distortion rate curve of the no-load B-EMF under different skew degree

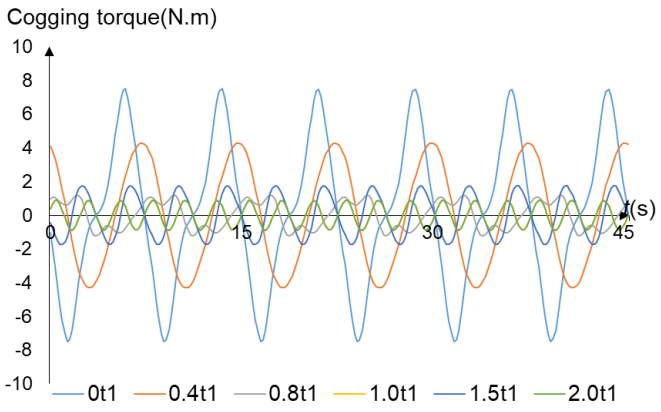

Fig. 7. Cogging torque waveform corresponding to part of the skew scheme

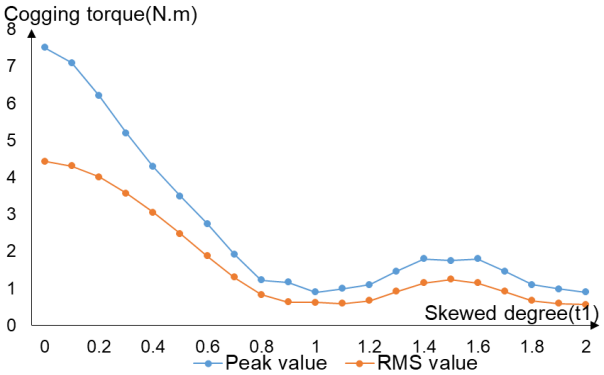

Fig. 8. Peak cogging torque and RMS value curves under different skew degree

skew degree (that is, the waveform quality continues to improve). Specifically, in the interval of a skew degree of $0 - 1t_1$, the decline is obvious, and in the interval of a skew degree of $1 - 2t_1$, the downward trend gradually slows down.

2. From the instantaneous value curve of cogging torque, as shown in Fig. 7, we can see that the overall trend of cogging torque is declining. Judging from the cogging torque waveform, as shown in Fig. 8, the maximum value and root mean square (RMS) value curve, the restraint effect of the stator slot skew on it is quite significant. Moreover, the above two parameters have the minimum value when the skew angle is t_1 and $2t_1$. Among them, the peak value dropped from 7.50 N·m to 0.89 N·m, and the root mean square value dropped from 4.42 N·m to 0.59 N·m.

In order to reveal the cause of the above trend, Fourier decomposition was carried out on the no-load B-EMF waveform and the cogging torque waveform, and then observed: For the no-load B-EMF waveform, the 3rd, 9th, 11th, and 13th harmonics are relatively prominent; for the cogging torque, the 6th, 12th, 18th, and 24th harmonics are relatively prominent. The details are shown in Fig. 9 and Fig. 10.

On this basis, the change curve of the above-mentioned main harmonic component with the increase of the degree of stator slot skew is obtained, as shown in Fig. 11 and Fig. 12.

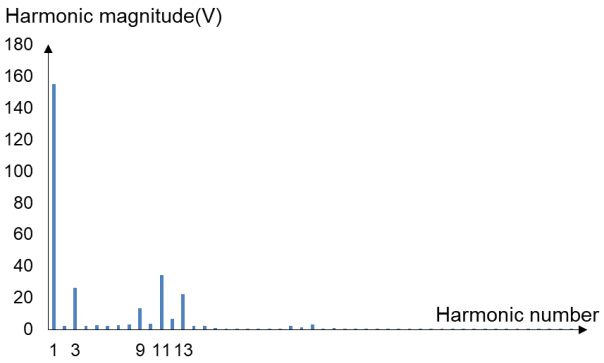

Fig. 9. Distribution of main harmonics component of no-load B-EMF

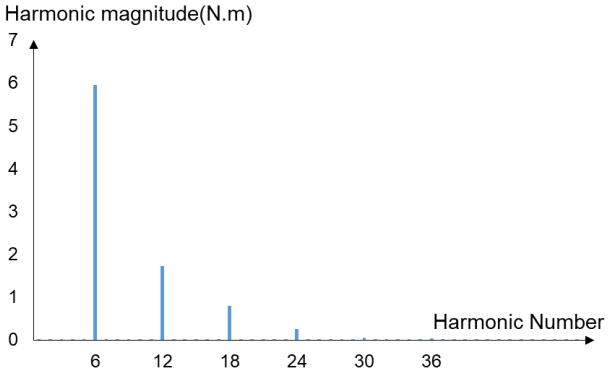

Fig. 10. Distribution of main harmonic order of cogging torque

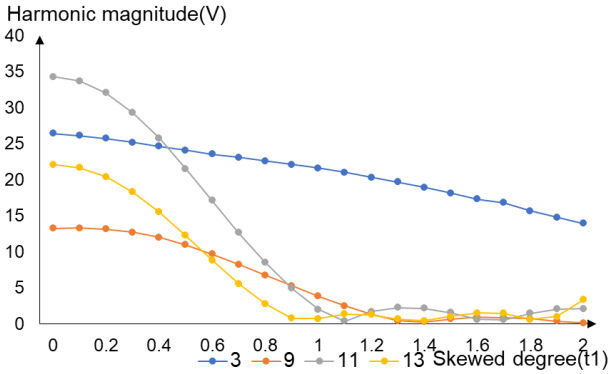

(a) Variation curve of main harmonic components of no-load B-EMF under different skew degrees

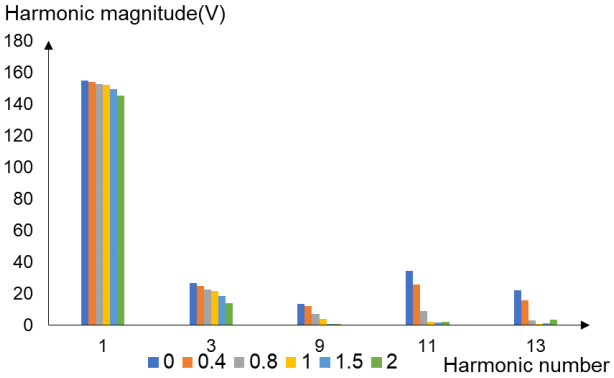

(b) Comparison of main harmonic components of no-load B-EMF of part of the skew structure

Fig. 11. The main harmonics component of no-load B-EMF change curve under different skew degrees

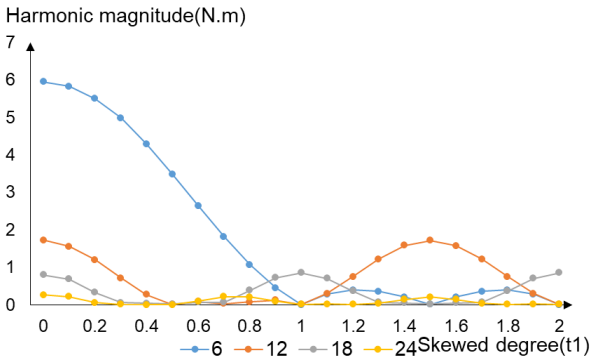

(a) Variation curve of main harmonic components of cogging torque under different skew degrees

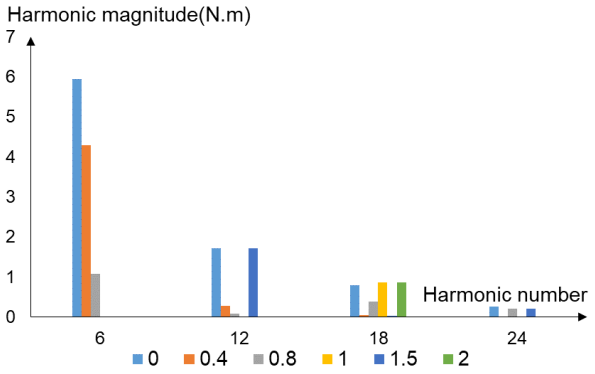

(b) Comparison of main harmonic components of cogging torque of part of the skew structure

Fig. 12. The main harmonic component of cogging torque varies under different skew degrees

From the above harmonic curve and graph, we can see:

1. As the degree of the stator slot skew increases, the main harmonic components of the no-load electromotive force are gradually reduced, as shown in Fig. 11(a) and Fig. 11(b), and the above changes have led to the changing trend of the sinusoidal distortion rate of the no-load induced electromotive force waveform as shown in Fig. 5.

2. As the degree of the stator slot skew increases, the main harmonics of cogging torque are effectively weakened, as shown in Fig. 12(a) and Fig. 12(b). At the same time, it should be noticed that when the stator slot skew structure exceeds 1 slot angle, the 12th harmonic will rebound to some extent. Therefore, from the principle of harmonic synthesis, the above-mentioned changes have led to the changing trend of the cogging torque peak value and the RMS value parameter as shown in Fig. 8.

3.3. Influence of other electromagnetic performance for stator slot skew structure

Under different stator slot skew degrees, the change trends of the electromagnetic torque, torque ripple, electromagnetic iron loss, electromagnetic power, and operating efficiency of the motor are shown in Figs. 13–18.

It can be seen from the above results:

1. As far as the waveform of the electromagnetic torque is concerned, its overall declines with the increase of the stator slot skew degree. When the stator slot skew degree is between $0-1t_1$, the RMS value of electromagnetic torque decreases relatively smoothly; when the stator slot skew degree is between $1.1-2t_1$, the decreasing trend is relatively significant, as shown in Fig. 13. As a result, when the skew degree is more than t_1, the quality of electromagnetic toque will be largely deteriorated.

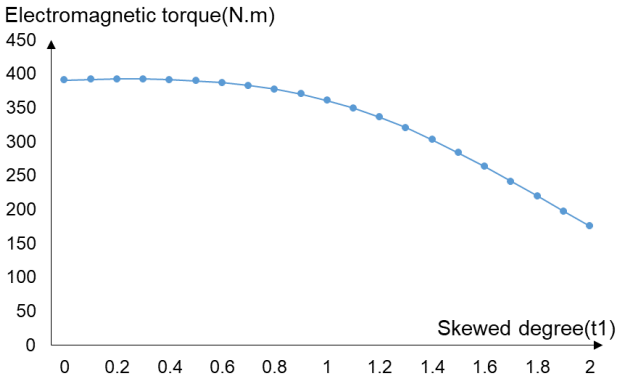

Fig. 13. RMS curve of electromagnetic torque corresponding to different skew degrees

What's more, less torque ripple means that the motor will have smaller vibration and noise. The electromagnetic torque ripple decreases between $0-t_1$ but increases between t_1-t_2, which reaches the minimum value when the stator slot skew degree is $1t_1$, and is only 4.12%, as shown in Fig. 14. Therefore, the best skew degree for torque ripple is t_1.

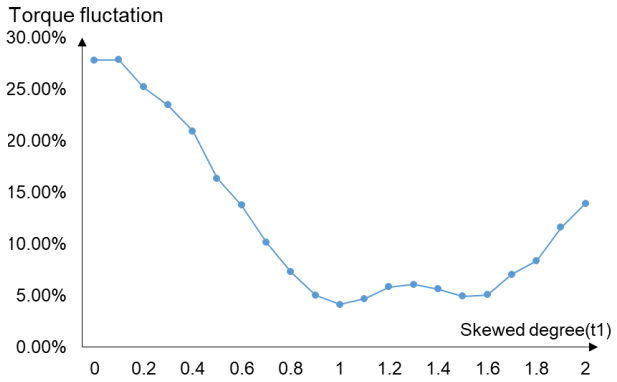

Fig. 14. Electromagnetic torque fluctuation curve corresponding to different skew degrees

2. As for the loss, this paper focuses mostly on the iron loss and permanent magnets loss. The stator slot skew structure has a significant weakening effect on the motor iron loss, and when the skew degree is an integer multiple of t_1, the iron loss takes the minimum value, as shown in Fig. 15. Meanwhile, the loss of permanent magnets increases with the increase of the stator slot skew degree, which would result in the increasing risk of demagnetization at elevated temperature, as shown in Fig. 16.

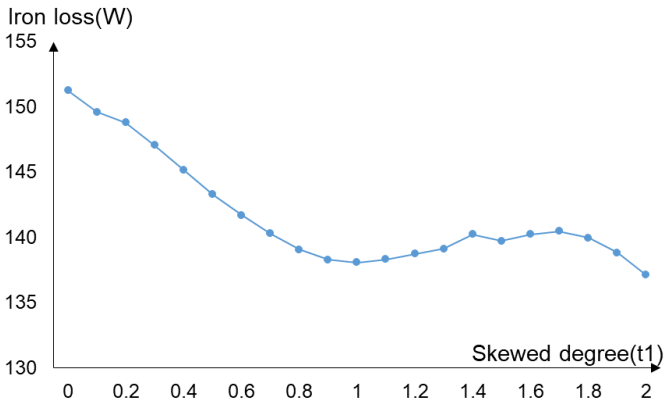

Fig. 15. Iron loss curve corresponding to different skew degrees

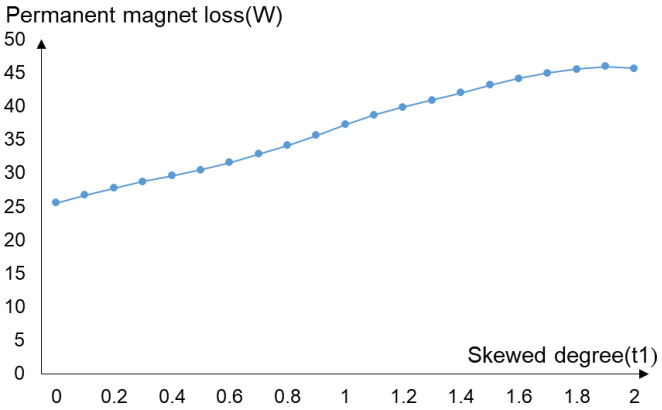

Fig. 16. Permanent magnet loss curve corresponding to different skew degrees

3. The input, output power, and motor operating efficiency waveforms have the same change trend, which have a relatively gentle downward trend when the stator slot skew degree is between $0-1t_1$, but they decrease significantly when the stator slot skew degree is between $1.1-2t_1$, as shown in Fig. 17 and Fig. 18.

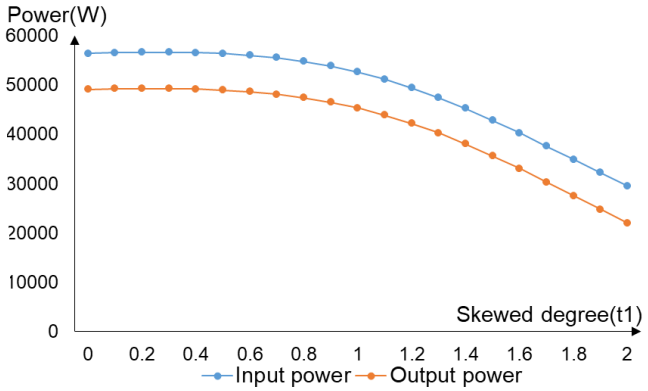

Fig. 17. Input and output power curves corresponding to different skew degrees

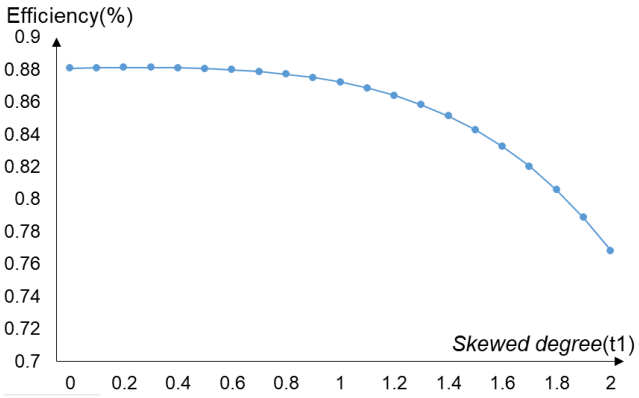

Fig. 18. Curves of operating efficiency corresponding to different skew degrees

4. Conclusions

1. The stator slot skew structure can effectively reduce the waveform distortion rate of the no-load B-EMF and cogging torque. The main reason is that this structure can effectively weaken the main harmonic components of the above two electromagnetic performances. Moreover, when the stator slot skew degree is 1 and 2 per stator slot pitch, the optimization effect on the no-load B-EMF waveform and cogging torque is more obvious.
2. The stator slot skew structure can reduce the electromagnetic torque ripple of the motor, and the torque ripple is the smallest when the skew angle is 1 per stator slot pitch.
3. The stator slot skew structure can weaken the electromagnetic torque, input power, output power and operating efficiency, and when the stator slot skew degree is between 0 – 1 per stator slot pitch, the drop amplitude is much less; when the stator slot skew degree is between 1 – 2 per stator slot pitch, the above-mentioned parameters drop more drastically.

4. The iron loss of this type of motor is smaller when the stator slot skew degree is 1 or 2 per stator slot pitch, and the permanent magnet loss will increase with the increase of the skew degree.
5. Based on the above results, it can be considered that for this type of motor, under the condition that the stator input current is constant, the relatively good value range of the stator slot skew degree should be about 1 per stator slot pitch.

Compared to the conventional design of this motor, this paper proposes a relatively more accurate optimum design of stator slot skew structure through a comparison of the above electromagnetic performance parameters. This paper has a certain reference value for the design, manufacturing, operation and maintenance, maintenance and protection levels to enhance such permanent magnet brushless DC motors.

Acknowledgements

This work was sponsored by the National Natural Science Foundation (Youth Foundation) of China, No. 51607146, and Sichuan Science and Technology Program, No. 2018GZ0391, as well as Sichuan Hydropower Energy and Power Equipment Technology Engineering Research Center, Xihua University, Chengdu, China, under Grant SDNY2020-001. Altair provides FLUX software support.

References

[1] Zhang Chen, *Principle and Application of Brushless DC Motor*, China Machinery Industry Press, Beijing (1996).

[2] Tang Renyuan, *Modern Permanent Magnet Motor Theory and Design*, Mechanical Industry Press, Beijing (2005).

[3] Li Weiqi, Lin Rongwen, Tao Tao, *Optimized design based on the air gap length of the built-in permanent magnet brushless DC motor*, Electric Switchgear, vol. 58, no. 05, pp. 58–63 (2020).

[4] Parsa L., Hao L., *Interior Permanent Magnet Motors with Reduced Torque Pulsation*, IEEE Transactions on Industrial Electronics, vol. 55, no. 2, pp. 602–609 (2008), DOI: 10.1109/TIE.2007.911953.

[5] Ren Dejiang, Huang Qu, Li Jianjun, Wu Ning, *Cogging torque optimization analysis of built-in permanent magnet synchronous motor*, Explosion-Proof Electric Machine, vol. 54, no. 4, pp. 4–7+43 (2019).

[6] Zhao W., Lipo T.A., Kwon B., *Torque Pulsation Minimization in Spoke-type Interior Permanent Magnet Motors with Skewing and Sinusoidal Permanent Magnet Configurations*, IEEE Transactions on Magnetics, vol. 51, no. 11, pp. 1–4 (2015), DOI: 10.1109/TMAG.2015.2442977.

[7] Aimeng W., Heming L., Weifu L., Haisen Z., *Influence of skewed and segmented magnet rotor on IPM machine performance and ripple torque for electric traction*, IEEE International Electric Machines and Drives Conference, pp. 305–310 (2009), DOI: 10.1109/IEMDC.2009.5075222.

[8] Adrian Młot, Marcin Kowol, Janusz Kołodziej, Andrzej Lechowicz, Piotr Skrobotowicz, *Analysis of IPM motor parameters in an 80-kW traction motor*, Archives of Electrical Engineering, vol. 69, no. 2 (2020), DOI: 10.24425/aee.2020.133038.

[9] Yang Zhihao, Yang Mengxue, Wang Sinuo, Bao Xiaohua, *The influence of stator skew on the performance of permanent magnet synchronous motors*, Transactions of the Chinese Society of Electrical Engineering, vol. 14, no. 3, pp. 97–102 (2019).

[10] Wang Dongliang, Chen Wei, *Discussion on the electromagnetic design of concentrated winding permanent magnet motor from the perspective of torque fluctuation*, Electric Tool, vol. 4, pp. 15–17 (2017), DOI: 10.16629/j.cnki.1674-2796.2017.04.004.

[11] Xiaodong S., Zhou S., Long C., Zebin Y., *Skew Angle Optimization Analysis of a Permanent Magnet Synchronous Motor for EVs*, IEEE International Conference on Applied Superconductivity and Electromagnetic Devices (ASEMD), pp. 1–2 (2018), DOI: 10.1109/ASEMD.2018.8558826.

[12] Wang Changcheng, Guo Hui, Sun Pei, Liu Ningning, Wang Yansong, Qin Yifei, *A method for reducing cogging torque of permanent magnet synchronous motors*, Light Industry Machinery, vol. 36, no. 6, pp. 62–66 (2018).

[13] He Qiang, *Magnetic field analysis and cogging torque study of brushless DC permanent magnet motors*, Hefei University of Technology (2016).

[14] Hongwei Fang, Hongxu Chen, *Analysis and reduction of the cogging torque of flux-modulated generator for wave energy conversion*, Energy Procedia, vol. 158, pp. 327–332 (2019), DOI: 10.1016/j.egypro.2019.01.097.

[15] Fu Lixin *et al*., *GB/T 1029-2005 Three-phase synchronous motor test method*, China Standard Press, Beijing (2006).